Embedded energy state in an open semiconductor heterostructure

Ivana Hrebikova[*] and Lukas Jelinek[†]

Department of Electromagnetic Field, Faculty of Electrical Engineering, Czech Technical University in Prague,
166 27 Prague, Czech Republic

Mário G. Silveirinha[‡]

Department of Electrical Engineering, Instituto de Telecomunicações, University of Coimbra, 3030-290 Coimbra, Portugal

In this paper, we show that HgCdTe heterostructures may support, within the envelope function approximation, bound electronic states embedded in the continuum, such that the discrete energy spectrum overlaps the continuous spectrum. Although the proposed heterostructures are generally penetrable by an incoming electron wave, it is shown that they may support spatially localized trapped stationary states with an infinite lifetime. We discuss the possibility of a free electron being captured by the proposed open resonator and present a detailed study of the trapping lifetime in the case of a detuned resonator.

I. INTRODUCTION

The stationary states of a quantum system with a finite-height potential well are commonly divided into bound states, which form a discrete spectrum, and unbound states, which form a continuum [1]. Usually, the two classes of modes do not overlap: the energies of the bound states usually lie within a potential well, while the energies of the unbound states lie above the potential well. Surprisingly, this property of a quantum system is not universal, as there are theoretical predictions of systems with bound-state energies falling into the continuum, so-called bound states in the continuum (BICs). Pioneering work pointing out that bound states with energies in the continuum are exact solutions of the one-electron Schrödinger equation for specific potentials was presented by von Neumann and Wigner in 1929 [2]. That paper also showed how to design electric potentials supporting BICs. The original formulation of von Neumann and Wigner has been reworked and even extended to a two-electron wave function [3], still bearing the sign of BICs. More recently, it has been proposed that the BICs can be decoupled from all continuum states also by virtue of symmetry [4–6].

Alongside the paradigm introduced above, the so-called resonant states in quantum systems have been discovered [7]. These represent a different approach for achieving "bound" states (resonances) with energies lying above the continuum threshold. These narrow-width resonances were proposed to exist as metastable states trapped by a large potential barrier or as quasibound states in closed channels of a system with weakly coupled channels [8–10]. Strictly speaking, however, these states are not truly bound, as they are, in fact, localized states with a finite lifetime constructed from continuum states. Their appearance is, however, very close to true BICs.

The experiment closest to observing BICs was carried out by Capasso *et al.* in 1992 [11]. The bound state, albeit with energy above the potential barrier, was *de facto* a defect

mode achieved by Bragg reflections in the periodic system of potential wells [12]. Another similar experiment, where the bound states were coupled to the continuum, was the case of (Ga, In)(As, N)/(Al, Ga)As quantum wells done by Albo *et al.* [13].

The resonant states in the continuum have recently elicited significant interest in the field of photonics. Indeed, for light waves it may be easier to design a resonator environment at will, using photonic crystals or metamaterials [14–18]. Photonic crystals even made an experimental observation of BICs possible [19–21]. In this context, BICs may be regarded as limiting cases of leaky waves. The usual leaky-wave states discussed in the electromagnetism literature are excitations with a finite lifetime and are in some sense the analog of electronic "resonant states." Thus, a BIC may be seen as the limit of a leaky state with vanishingly small resonance width [21–23].

Until recently, all the known realizations of BIC resonators required infinitely extended material profiles, e.g., a photonic crystal. Truncation of the material profile leads to imperfect localization and to finite oscillation lifetimes. Importantly, however, it was shown in Ref. [17] that spatially unbounded resonators are not required to have BICs and that, under some strict conditions, volume plasmons may enable the formation of BICs in open cavities of finite size.

In this paper we propose a semiconductor heterostructure supporting BICs, although it is characterized by a potential well of finite height. Inspired by Ref. [17] and using an electron-light-wave analogy, we show that an electron can be trapped with an infinite lifetime within a spherical core-shell heterostructure when the electron dispersive mass in the shell is precisely zero and the radius of the core is precisely tuned. All results are based on an effective-medium approximation [24].

II. A CORE-SHELL TRAP FOR ELECTRONS

A. Electron-light analogy

The trapped electron states in a crystalline heterostructure are determined by the microscopic time-independent

───────
[*]hrebiiva@fel.cvut.cz
[†]lukas.jelinek@fel.cvut.cz
[‡]mario.silveirinha@co.it.pt

Schrödinger equation

$$-\frac{\hbar^2}{2m_e}\Delta\psi_{mic}(\mathbf{r}) + V_{mic}(\mathbf{r})\psi_{mic}(\mathbf{r}) = E\psi_{mic}(\mathbf{r}), \quad (1)$$

where Δ is the Laplacian operator, $\psi_{mic}(\mathbf{r})$ is the wave function of an electron from the top energy shells, E is energy, and $V_{mic}(\mathbf{r})$ is the effective microscopic potential associated with the ion lattice of period a and with the rest of the electrons [25].

In realistic heterostructures, where each layer is composed of many atoms and the wave vectors of the electron are small $k \ll 2\pi/a$, the description of the valence electrons can, however, be further simplified. In such a case, it is possible to homogenize the microscopic wave function $\psi_{mic}(\mathbf{r})$ and the potential $V_{mic}(\mathbf{r})$ [26–28], resulting in an effective "macroscopic" wave function $\psi_{eff}(\mathbf{r}) = \langle\psi_{mic}\rangle$, which varies slowly on the scale of the lattice constant, and in an effective potential $V_{eff}(\mathbf{r}) = \langle V_{mic}\rangle$, which is a constant for each heterostructure layer [26–31]. The brackets $\langle\cdot\rangle$ represent the operation of spatial averaging. This *envelope function* formalism was originally introduced by Bastard [24,27,32], and it was further reworked in recent studies [28,30,31]. The point of view of this paper is based on the ideas of Refs. [28,31].

An important observation is that $\psi_{eff} = \langle\psi_{mic}\rangle$ does not imply that $|\psi_{eff}(\mathbf{r})|^2 = \langle|\psi_{mic}|^2\rangle$, and hence $|\psi_{eff}(\mathbf{r})|^2$ does not generally represent the probability density. The spatially averaged probability density of energy eigenstates can be written in terms of ψ_{eff} as [28,29,33] (see the Appendix)

$$\langle|\psi_{mic}|^2\rangle = \left(1 - \frac{\partial V_{eff}}{\partial E}\right)|\psi_{eff}|^2 + \frac{\hbar^2}{m^2}\frac{\partial m}{\partial E}\|\nabla\psi_{eff}\|^2. \quad (2)$$

Within this paradigm, the wave function ψ_{eff} satisfies the macroscopic time-independent Schrödinger equation

$$-\frac{\hbar^2}{2m}\Delta\psi_{eff}(\mathbf{r}) + V_{eff}\psi_{eff}(\mathbf{r}) = E\psi_{eff}(\mathbf{r}), \quad (3)$$

where $V_{eff} = E_{\Gamma_6}$ is the band-edge energy of the conduction (Γ_6) band and where m is dispersive mass [26–28,31], defined as

$$\frac{1}{m} = \frac{1}{m_e} + v_P^2\left(\frac{2}{E - E_{\Gamma_8}} + \frac{1}{E - E_{\Gamma_7}}\right). \quad (4)$$

Here, $v_P^2 = 2P^2/3\hbar^2$, and P is Kane's parameter [26], which determines the curvature of the bands. The energy E_{Γ_8} is the band-edge energy of the valence band, and the energy E_{Γ_7} is the band-edge energy of the spin-orbit split-off band. The dispersive mass depends on the electron energy, and in general, it differs from the effective mass calculated from the curvature of the band structure.

To ensure that the wave function $\psi_{eff}(\mathbf{r})$ follows the relevant physics at the interfaces of the layers, Eq. (3) is further complemented with boundary conditions, i.e., with the continuity of ψ_{eff} and $\partial_n\psi_{eff}/m$ at each boundary, where $\partial_n = \partial/\partial n$ and n represents the direction normal to the boundary surface [24,31]. For convenience, we introduce the function $\tilde{\psi}_{eff}(\mathbf{r}) = \psi_{eff}(\mathbf{r})/m$, which proves useful for handling the limit $m \to 0$ ($E = E_{\Gamma_8}$), which will be discussed later. Note that the boundary conditions satisfied by $\tilde{\psi}_{eff}$ are the continuity of $m\tilde{\psi}_{eff}$ and the continuity of $\partial_n\tilde{\psi}_{eff}$.

In this paper, we consider heterostructures with spherical symmetry (each heterostructure layer is a spherical shell). In

such a case, one can look for a solution of Eq. (3) of the form $\tilde{\psi}_{eff}(\mathbf{r}) = \tilde{R}_l(r)P_l(\cos\theta)$, where $P_l(\cos\theta)$ represents a Legendre polynomial of order l [34]. It is straightforward to show [34] that the time-independent Schrödinger equation reduces to

$$\frac{1}{r^2}\frac{\partial}{\partial r}\left[r^2\frac{\partial\tilde{R}_l}{\partial r}\right] + \left[\frac{2m}{\hbar^2}(E - E_{\Gamma_6}) - l(l+1)\frac{1}{r^2}\right]\tilde{R}_l = 0. \quad (5)$$

Due to the orthogonality of the Legendre polynomials and the spherical symmetry of the system, the boundary conditions for $\tilde{\psi}_{eff}(\mathbf{r})$ reduce to the continuity of $m\tilde{R}_l(r)$ and $\partial_r\tilde{R}_l(r)$ at each heterostructure boundary.

Unlike an electron in a crystalline heterostructure, a light bound mode in an electromagnetic heterostructure is described by a vector wave equation. In general, the vector wave equation does not reduce to three uncoupled scalar equations, so there is no immediate analogy between the light case and the electron wave case. In the case of spherical coordinates [34], the electromagnetic fields can fortunately be separated into transverse electric radial TE^r waves and transverse magnetic radial TM^r waves (transverse with respect to the radial direction) [35]. The TE^r waves can be derived from a single component of the electric vector potential $\mathbf{F} = \hat{\mathbf{r}}F_r$, and the TM^r waves can be derived from a single component of the magnetic vector potential $\mathbf{A} = \hat{\mathbf{r}}A_r$, so that the vector wave equation reduces to a scalar wave equation [35, pp. 553–557].

$$(\Delta + k^2)\frac{F_r}{r} = 0, \quad (6a)$$

$$(\Delta + k^2)\frac{A_r}{r} = 0. \quad (6b)$$

By analogy with the electronic case, we introduce auxiliary functions $\tilde{F}_r = F_r/\mu r$ and $\tilde{A}_r = A_r/\varepsilon r$, so that the wave equations (6a) and (6b) are further complemented by boundary conditions that impose the continuity of $\mu\tilde{F}_r$ and $\partial_r\tilde{F}_r$ for the TE^r waves and the continuity of $\varepsilon\tilde{A}_r$ and $\partial_r\tilde{A}_r$ for the TM^r waves, where ε and μ are the permittivity and the permeability, respectively.

By comparing (3) and (6a) and (6b) and the corresponding boundary conditions, a direct analogy between the semiconductor and the electromagnetic cases is obtained (see Table I).

Table I also reveals that the presented electron-light analogy for spherical waves is very similar to that for plane waves [36–39].

TABLE I. The analogy between an electron wave and electromagnetic waves.

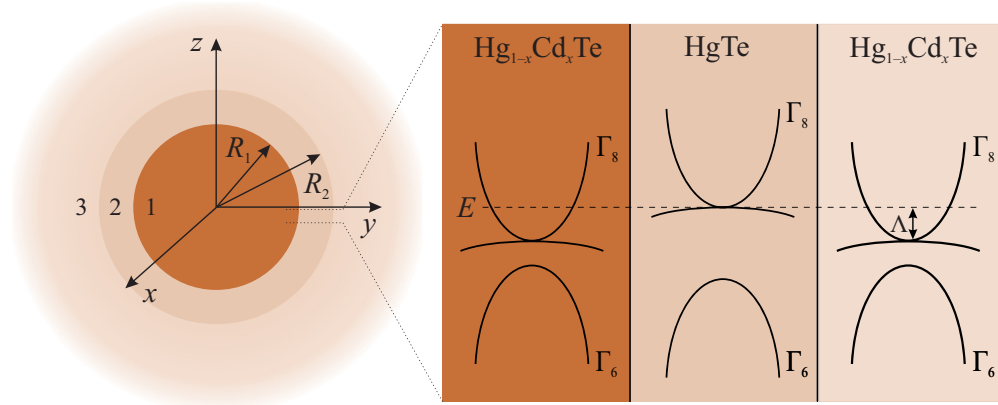| Electron wave	TE wave	TM wave
$\tilde{\psi}_{eff} = \psi_{eff}/m$	$\tilde{F}_r = F_r/\mu r$	$\tilde{A}_r = A_r/\varepsilon r$
m	μ	ε
$2(E - E_{\Gamma_6})$	ε	μ
$k^2 = \frac{2m(E-E_{\Gamma_6})}{\hbar^2}$	$\omega^2\varepsilon\mu$	$\omega^2\varepsilon\mu$
$\Delta f + k^2 f = 0, f = \{\tilde{\psi}_{eff}, \tilde{F}_r, \tilde{A}_r\}$		
Continuity		
$m\tilde{\psi}_{eff}$	$\mu\tilde{F}_r$	$\varepsilon\tilde{A}_r$
$\partial_r\tilde{\psi}_{eff}$	$\partial_r\tilde{F}_r$	$\partial_r\tilde{A}_r$

FIG. 1. (Color online) (left) A sketch of an open core-shell resonator for electrons consisting of a core with radius R_1 and a shell of width $R_2 - R_1$. The core-shell structure is surrounded by an infinite background material. (right) A sketch of the energy band structures of the heterostructure. The energy level associated with the embedded energy state is represented by a dashed horizontal line and corresponds to the edge of the valence (Γ_8) band of HgTe. Number 1 denotes the core, number 2 denotes the shell, and number 3 denotes the background. Note that the considered semiconductor compounds have an inverted band structure, such that the order of the valence band Γ_8 and of the conduction band Γ_6 is reversed.

B. The embedded eigenstate

The idea of a trapped electron is inspired by the electromagnetic case [17], where it was shown that electromagnetic modes can under certain conditions be bound with infinite lifetimes in a core-shell nanoparticle. Particularly, the TM^r modes can be bound in the inner region of a core-shell nanostructure when the permittivity of the shell is zero valued, $\varepsilon_{\text{shell}} = 0$, and the radius of the core has a precise value. In such a case, the shell has infinite transverse wave impedance and behaves, for this particular mode of oscillation, as a perfect magnetic conductor (PMC).

Applying the analogy described in the previous section, we see that an electron may be trapped in the core of a spherical heterostructure with an energy such that the dispersive mass of the shell vanishes. From Eq. (4) the condition $m = 0$ is satisfied for an energy such that $E = E_{\Gamma_8}^{(2)}$, i.e., at the edge of the valence (with p-type symmetry) band. In what follows, we will show that a semiconductor with a zero-valued dispersive mass may, indeed, effectively behave as an infinite barrier for the electron and enables the emergence of a spatially localized stationary state embedded within the continuum. The geometry of the open quantum resonator is sketched in Fig. 1.

Our design is based on the ternary compound Hg$_{1-x}$Cd$_x$Te, with x being the mole fraction of cadmium [40]. This ternary compound is used mainly because of its favorable valence-band offset values and due to the nearly perfect lattice matching between HgTe and CdTe.

In our design, both the core (Hg$_{0.9}$Cd$_{0.1}$Te) and the shell (HgTe) have inverted band structures with the Γ_8 bands lying above the Γ_6 bands (Fig. 1), and the core and the background materials are assumed to be identical. The fact that the semiconductor compounds have inverted band structures, and thus a negative dispersive mass within the band gap, does not play any role in the context of the emergence bound states embedded in the continuum. In principle, BICs can also be supported by other semiconductors with regular band structure. The band-edge energies are calculated from the width of the band gap $E_g = E_{\Gamma_6} - E_{\Gamma_8}$ and from the

split-off energy $\Delta = E_{\Gamma_8} - E_{\Gamma_7}$. Energy E_g is computed from Hansen's formula [40], considering zero temperature. The split-off energy is taken as $\Delta = 0.93$ eV [41]. The valence-band offset between HgTe and Hg$_{1-x}$Cd$_x$Te (see Fig. 1) is evaluated as $\Lambda = 0.35x$ eV [42]. Kane's parameter P is given by the relation $2P^2 m_e / \hbar^2 = 18 + 3x$ eV [43].

Next, we formally demonstrate that Eq. (5) supports a bound state when $E = E_{\Gamma_8}^{(2)}$, i.e., when $m_2 = 0$ in the shell. Note that the energy level $E = E_{\Gamma_8}^{(2)}$ lies within the continuous energy spectrum of the background and core regions (Fig. 1), so the wave number $k_1 = \sqrt{2m_1(E - E_{\Gamma_6}^{(1)})/\hbar^2}$ in the core and background regions is real valued. Under the assumptions that $m_2 = 0$ in the shell and that the wave function vanishes in the background region, the solution of the radial part of the Schrödinger equation (5) can be written in the form [34]

$$\tilde{R}_l(r) = N_0 \begin{cases} j_l(k_1 r) & r < R_1, \\ A_l(k_1 r)^l + B_l(k_1 r)^{-l-1} & R_1 < r < R_2, \\ 0 & r > R_2, \end{cases} \quad (7)$$

where N_0 is a normalization constant. The unknown coefficients A_l and B_l are determined by the boundary conditions, which require the continuity of $m\tilde{R}(r)$ and $\partial_r \tilde{R}(r)$ at the two interfaces. The continuity of $\partial_r \tilde{R}(r)$ implies that coefficients A_l and B_l are related as

$$A_l = \frac{(k_1 R_1)^{1-l}}{l} j_l'(k_1 R_1) \left[1 - \left(\frac{R_2}{R_1} \right)^{2l+1} \right]^{-1} \quad (8)$$

and

$$B_l = A_l \frac{l}{l+1} (k_1 R_2)^{2l+1}, \quad (9)$$

where $j_l'(x) = \partial j_l(x) / \partial x$.

The continuity of $m\tilde{R}(r)$ imposes that the inner radius must satisfy
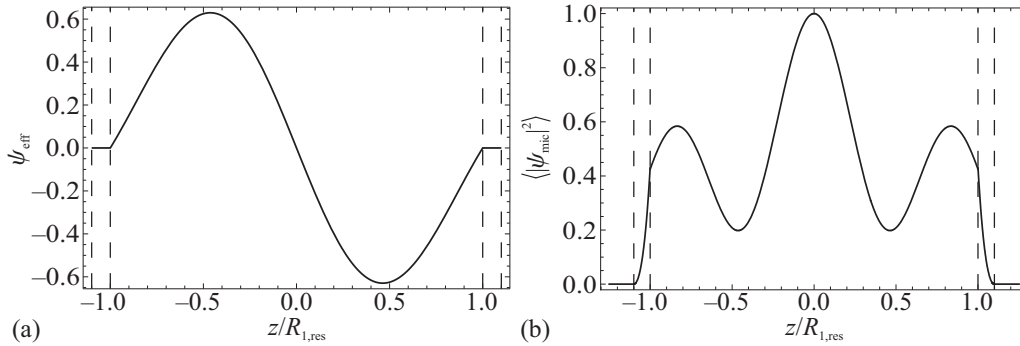
$$j_l(k_1 R_1) = 0. \quad (10)$$

FIG. 2. (a) The macroscopic wave function ψ_{eff} and (b) the spatial average probability density $\langle|\psi_{\text{mic}}|^2\rangle$ (normalized to the peak value) of the trapped electron as a function of the normalized z coordinate.

This condition shows that in order to have an embedded energy eigenvalue, the radius of the core region must be chosen precisely. For $l = 1$ (dipole-type symmetry) this condition implies that the smallest possible radius for the core is $R_{1,\text{res}} \approx 4.49/k_1$. This analysis confirms the hypothesis that the electron can be trapped in the core of the semiconductor heterostructure if the dispersive mass of the shell is zero valued and the radius of the core has a very specific value.

It is important to highlight the following:

(i) In the ideal case of $m_2 = 0$, the resonance condition is independent of the shell thickness.

(ii) For $l = 0$, the calculated coefficients A_l and B_l are singular, and hence a wave function with monopole (s-type orbital) symmetry cannot be trapped within the core. This important result implies that our resonator is penetrable by electron waves with monopole symmetry; that is, a semiconductor with a zero-valued dispersive mass behaves as an infinite barrier only for waves with a nonzero azimuthal quantum number. Thus the core-shell heterostructure is generally open to electron waves. This is similar to the electromagnetic case, where a TM^r wave may be bound to the core by a shell made of permittivity near zero (ENZ) material, with the shell being penetrable by TE^r waves [17].

(iii) The trapped modes are degenerate because for each l there are in total $2l + 1$ spherical harmonics differing only in the magnetic quantum number [34].

To illustrate the proposed theory, we consider a semiconductor heterostructure with an HgTe shell. The Hg$_{1-x}$Cd$_x$Te core has mole fraction $x = 0.1$ and radius $R_1 = R_{1,\text{res}} \approx 4.49/k_1 \sim 65a$, where $a = 0.65$ nm is the lattice constant of the considered bulk semiconductor alloys. The radius of the shell is $R_2 = 1.1 R_{1,\text{res}}$. The trapped electron state has dipole-type symmetry ($l = 1$).

The calculated radius dependence of the "macroscopic" wave function ψ_{eff} and the corresponding averaged probability density $\langle|\psi_{\text{mic}}|^2\rangle$ along the z axis are depicted in Fig. 2. Note that (2) allows for writing $\langle|\psi_{\text{mic}}|^2\rangle$ in terms of $\tilde{\psi}_{\text{eff}}$ as follows:

$$\langle|\psi_{\text{mic}}|^2\rangle = m^2|\tilde{\psi}_{\text{eff}}|^2 + \hbar^2 \frac{\partial m}{\partial E}\|\nabla\tilde{\psi}_{\text{eff}}\|^2. \quad (11)$$

To obtain the formula presented above, we used $\partial V_{\text{eff}}/\partial E = 0$. It is interesting to note that for both semiconductor alloys $m \approx (E - E_{\Gamma_8})/2v_P^2$ in the energy range of interest, with $v_P^2 = 2P^2/3\hbar^2$ [28]. The parameter v_P has units of velocity. Thus

$\partial m/\partial E \approx 1/2v_P^2$, which is approximately the same in both the core and the shell.

Figure 2(a) shows that the macroscopic electron wave function is entirely confined within the core; that is, ψ_{eff} is identically zero not only outside the core-shell resonator but also in the shell. However, as shown in Fig. 2(b), the average probability density has a symmetry different than the squared amplitude of the macroscopic wave function and furthermore is nonzero in the shell. This means that the microscopic wave function ψ_{mic} has strong fluctuations on the scale of the unit cell of the HgTe shell, so that its macroscopic spatial average vanishes in the shell, while the corresponding probability density function is nonzero. The fact that the probability of finding the electron in the shell is nonzero is consistent with the electromagnetic case, for which the electromagnetic energy stored in the ENZ shell is nonzero. Thus, a zero dispersive mass, $m_2 = 0$, and a nonzero azimuthal quantum number imply that the shell behaves as an infinite-height potential barrier that blocks the electron tunneling out of the resonator.

It is relevant to note that in the electromagnetic case the light remains confined in the core region due to the screening provided by the (nonradiative) volume plasmons of the shell [17]. Interestingly, in the semiconductor case studied here the role of the plasmons is played by the heavy-hole states of HgTe [44]. In our framework the heavy-hole states have a flat energy dispersion and occur precisely at the energy level wherein the dispersive mass vanishes.

C. Density of states

In order to further support the hypothesis of the emergence of the bound state in the continuum, the density of states in the background material has been evaluated as Ref. [45]

$$g(E) = \sum_n \frac{1}{(2\pi)^3}\int_{E=E_{n\mathbf{k}}} \frac{1}{|\nabla_{\mathbf{k}}E_{n\mathbf{k}}|}dS, \quad (12)$$

where the summation is over all bands. Accounting for a spin degeneration and realizing that the surfaces $E = E_{n\mathbf{k}}$ are spherical within the effective-medium model used, Eq. (12) can be simplified as

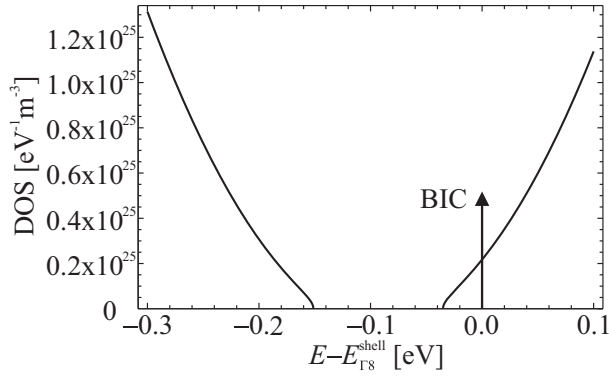$$g(E) = \frac{1}{\pi^2}\frac{k^2}{|\hbar v_g|}, \quad (13)$$

FIG. 3. Density of states in the background medium. The vertical arrow represents the bound state in the continuum.

where

$$v_{\rm g} = \frac{1}{\hbar}\frac{\partial E}{\partial k} = v_P \frac{\sqrt{\left(E - E_{\Gamma_6}\right)\left(E - E_{\Gamma_8}\right)}}{\left(E - \left(E_{\Gamma_6} + E_{\Gamma_8}\right)/2\right)} \qquad (14)$$

is the group velocity. It is important to note that Eq. (14) assumes the linear mass approximation $m \approx (E - E_{\Gamma_8})/2v_P^2$, which is valid in the vicinity of E_{Γ_8}.

From the dispersion of the energy stationary states it is possible to write the wave vector k as a function of the energy, so that we finally get

$$g(E) = \frac{\left[\left(E - E_{\Gamma_6}\right)\left(E - E_{\Gamma_8}\right)\right]^{1/2}\left|E - \left(E_{\Gamma_6} + E_{\Gamma_8}\right)/2\right|}{\pi^2 \hbar^3 v_P^3}. \qquad (15)$$

The density of states (13) is depicted in Fig. 3. It can be seen that it is nonzero at the energy $E = E_{\Gamma_8}^{(2)}$ associated with the BIC. This confirms that the discrete spectrum really overlaps the continuum spectrum. It is worth mentioning that the density

of states of the background region is coincident with the density of states of the continuous spectrum of the structure. This is due to a one-to-one correspondence between the plane-wave electronic states in the background unbounded region and the extended electronic states in the presence of the semiconductor heterostructure.

Note that the usual paradigm is that the bound states occur within the band gaps of the background material, different from Fig. 3. In the present example, it may be shown that there are no bound states in the band gap between the valence and conduction bands of the background region. This happens because the band gap of the shell overlaps the band gap of the background and of the core regions (Fig. 1).

III. THE TRAPPING LIFETIME FOR A DETUNED RESONATOR

The previous section dealt with the ideal case, where the energy of the trapped electron is equal to the band-edge energy $E_{\Gamma_8}^{(2)}$ and the inner radius is perfectly tuned to the value $R_{1,\rm res}$ defined by Eq. (10). Such perfect tuning is, however, unrealistic, and it is interesting to characterize the trapping lifetime when the inner radius R_1 is detuned.

In the detuned case, the solution of the radial equation (5) has to be searched in the form

$$\tilde{R}(r) = \begin{cases} a_l j_l(k_1 r) & r < R_1, \\ b_l^{(1)} j_l(k_2 r) + b_l^{(2)} y_l(k_2 r) & R_1 < r < R_2, \\ c_l h_l^{(1)}(k_3 r) & r > R_2, \end{cases} \qquad (16)$$

where j_l and y_l are the spherical Bessel functions of the first and second kinds, respectively, $h_l^{(1)}$ is the spherical Hankel function of the first kind, and $k_i = \sqrt{2m_i(E - E_{\Gamma_6}^{(i)})/\hbar^2}$ is the wave number in the ith layer. As in the previous section, the unknown coefficients a_l, $b_l^{(1)}$, $b_l^{(2)}$, and c_l are obtained from the boundary conditions discussed previously, which result in the following equation system:

$$\begin{pmatrix} j_l(k_1 R_1) & -\dfrac{m_2}{m_1}j_l(k_2 R_1) & -\dfrac{m_2}{m_1}y_l(k_2 R_1) & 0 \\[2mm] j_l'(k_1 R_1) & -\dfrac{k_2}{k_1}j_l'(k_2 R_1) & -\dfrac{k_2}{k_1}y_l'(k_2 R_1) & 0 \\[2mm] 0 & \dfrac{m_2}{m_1}j_l(k_2 R_2) & \dfrac{m_2}{m_1}y_l(k_2 R_2) & -\dfrac{m_3}{m_1}h_l^{(1)}(k_3 R_2) \\[2mm] 0 & \dfrac{k_2}{k_1}j_l'(k_2 R_2) & \dfrac{k_2}{k_1}y_l'(k_2 R_2) & -\dfrac{k_3}{k_1}h_l'^{(1)}(k_3 R_2) \end{pmatrix} \begin{pmatrix} a_l \\[2mm] b_l^{(1)} \\[2mm] b_l^{(2)} \\[2mm] c_l \end{pmatrix} = 0. \qquad (17)$$

In the detuned case, this homogeneous system (16) has a nontrivial solution only for complex energy values, $E = E_{\rm re} + iE_{\rm im}$, which correspond to the zeros of the matrix determinant. The imaginary part of the energy is associated with the decay time of the localized state, and nonzero $E_{\rm im}$ implies that the electron escapes from the resonator. The trapping lifetime can be defined as $\tau \sim \hbar/(-2E_{\rm im})$ [1]. The lifetime is independent of the origin of the energy scale. The trapping lifetime is shown in Fig. 4 as a function of relative detuning $R_1/R_{1,\rm res}$ for $R_2 = 1.1R_{1,\rm res}$. The calculation assumes that the core and the background are made of $Hg_{0.9}Cd_{0.1}Te$ and that the shell is HgTe.

IV. SCATTERING CROSS SECTION OF THE CORE-SHELL RESONATOR

Since the resonator may support a state with an infinite lifetime, it is natural to ask if it can capture a free-electron propagating in the background region. To investigate this possibility, we will now study the scattering of a plane electron wave by the core-shell resonator.

Because of the angular symmetry of the resonator, it can be assumed without loss of generality that the plane wave propagates along the z axis. This plane wave may be
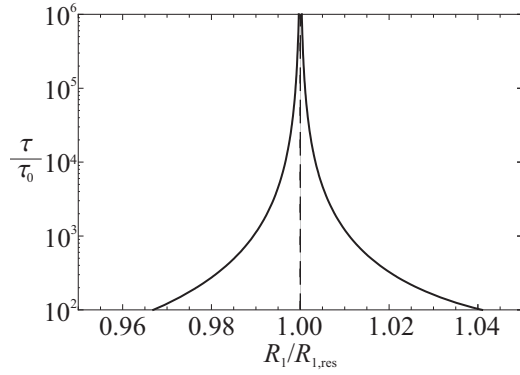
FIG. 4. The trapping lifetime as a function of relative detuning $R_1/R_{1,res}$. The trapping lifetime is normalized with respect to the time $\tau_0 = 2R_2/v_g = 0.11$ ps that the electron needs to pass the diameter of the core-shell resonator at the group velocity (14) in the background material. Note that the lifetime diverges to infinity for $R_1/R_{1,res} = 1$.

decomposed into Legendre polynomials as Ref. [46]

$$e^{ik_3z} = \sum_{l=0}^{\infty} i^l (2l+1) j_l(k_3 r) P_l(\cos\theta). \qquad (18)$$

This decomposition allows us to write the normalized wave function as $\tilde{\psi} = \sum_0^\infty \tilde{\psi}_l$, with $\tilde{\psi}_l(r,\theta,\varphi) = \tilde{R}_l(r) i^l (2l+1) P_l(\cos\theta)$ and

$$\tilde{R}_l(r) = \begin{cases} a_l j_l(k_1 r) & r < R_1, \\ b_l^{(1)} j_l(k_2 r) + b_l^{(2)} y_l(k_2 r) & R_1 < r < R_2, \\ c_l h_l^{(1)}(k_3 r) + j_l(k_3 r) & r > R_2. \end{cases} \qquad (19)$$

The unknown coefficients are obtained by imposing the previously discussed boundary conditions at the interfaces. Figure 5(a) shows the first four ($l = 0,1,2,3$) Mie scattering coefficients in the core region (a_l) as a function of the electron energy for a detuned resonator with $R_1 = 1.01 R_{1,res}$. The curve corresponding to $l = 0$ (black line) confirms that the heterostructure is penetrable by an electron wave with monopole symmetry. This is in conformity with the claim in Sec. II B. However, the remaining curves show clearly that a_l ($l \geqslant 1$) vanishes whenever $E = E_{ideal}$ [see Fig. 5(a)], where E_{ideal} is the valence-band-edge energy E_{Γ_8} of HgTe. For this

energy, the shell region behaves as an infinite height barrier, and the incident electron wave is unable to reach the core region. The most relevant of these coefficients, a_1, which is associated with the trapped state, is further studied in Fig. 5(b) for $R_1 \approx R_{1,res}$. In this case, our numerical simulations reveal that the approximation

$$a_1 \approx \frac{(E - E_{ideal})}{(E - E_{actual})} e^{i\phi_0} \qquad (20)$$

holds. In the above equation, E_{actual} is the complex-valued resonance energy determined by the inner radius R_1 which is calculated as explained in Sec. III, and ϕ_0 is some irrelevant phase factor. Notably, Eq. (20) and Fig. 5(b) reveal that in the limit case $R_1 \to R_{1,res}$ the zero associated with E_{ideal} cancels the pole corresponding to E_{actual}, and $|a_1| \to 1$. This contrasts with all the other a_l ($l \geqslant 2$), which in the present example vanish identically for $E = E_{ideal}$, regardless of the radius R_1. This means that, due to the cancellation of a zero pole, an incident wave with energy $E = E_{ideal}$ and dipole symmetry *may* actually penetrate into the shell, in the case of a perfectly tuned resonator [see Fig. 5(b), blue curve]. Nevertheless, even though the resonator may support an infinite-lifetime bound state and the free electron can penetrate into the core, it cannot be captured by the resonator.

Indeed, the condition for having a trapped electron in the present problem is that $|a_1| \to \infty$ for some real-valued E. It may be checked that even though $|a_1|$ can have rather large values in our structure, it remains finite for any real-valued energy. We therefore conclude that, in the scenario studied here, the resonator is unable to capture the free electron.

This discussion may suggest that it is impossible to couple a free electron to the embedded bound state. However, that is not necessarily the case. For example, if the resonator is perturbed during a short time period (e.g., by applying a time-varying electric or magnetic field), the temporary detuning may allow the free electron to excite the bound state and be permanently captured after the perturbation is removed. Another option is to excite another lower-energy filled bound state (part of the discrete spectrum) with an external field. These ideas will be explored in future work.
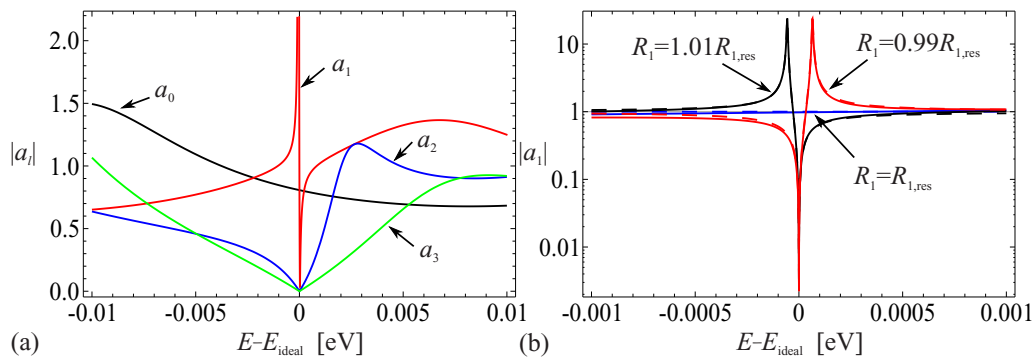

FIG. 5. (Color online) (a) Magnitude of the first four coefficients a_l ($l = 0,1,2,3$) as a function of relative energy detuning. The inner radius of the resonator is $R_1 = 1.01 R_{1,res}$. (b) Magnitude of a_1 as a function of relative energy detuning. The inner radius is $R_1 = \{0.99, 1, 1.01\} R_{1,res}$. The solid lines correspond to the exact solution, while the dashed lines correspond to the approximation (20).

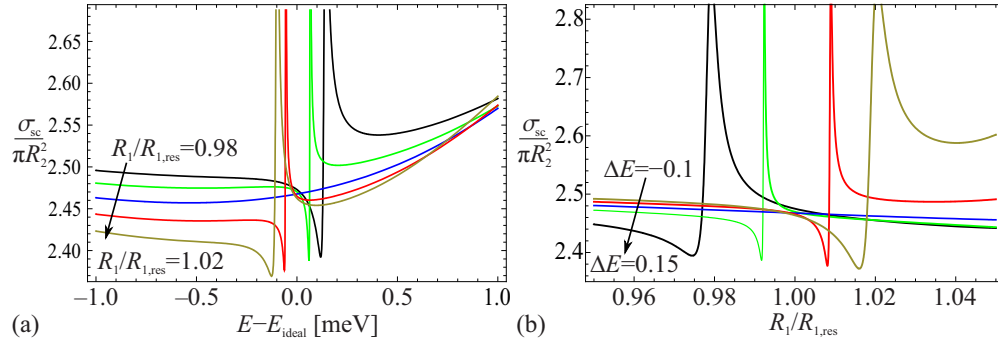FIG. 6. (Color online) (a) Scattering cross section σ_{sc} as a function of relative energy detuning for $R_1/R_{1,res} = 0.98, 0.99, 1, 1.01$, and 1.02. (b) Scattering cross section σ_{sc} as a function of the inner radius $R_1/R_{1,res}$ for incident electron energy $E = E_{ideal} + \Delta E$, where $\Delta E = \{-0.1, -0.05, 0, 0.1, 0.15\}$ meV. In all calculations the outer radius was taken as $R_2 = 1.1 R_{1,res}$.

It is also interesting to characterize the scattering cross section of the resonator. It is given by Ref. [47]

$$\sigma_{sc} = \int_\Omega \frac{\left| \psi_{sc} \frac{\partial \psi_{sc}^*}{\partial r} - \psi_{sc}^* \frac{\partial \psi_{sc}}{\partial r} \right| r^2}{|\psi_{inc} \nabla \psi_{inc}^* - \psi_{inc}^* \nabla \psi_{inc}|} d\Omega = \frac{4\pi}{k_1^2} \sum_l |c_l|^2 (2l+1),$$

(21)

where subscript sc stands for scattered and subscript inc stands for incident. Figure 6(a) shows that for a perfectly tuned resonator with $R_1 = R_{1,res}$ (blue curve), the scattering cross section does not exhibit any resonant features. This is consistent with the zero-pole cancellation discussed above. However, for a detuned inner radius R_1 there is a resonant response which indicates a strong interaction of the free-electron with the heterostructure because of temporary electron trapping. This behavior is also perceptible in Fig. 6(b), where the scattering cross section is represented for different energies of the incident electron.

V. CONCLUSION

It has been shown that a spherical semiconductor heterostructure may support bound states embedded within the continuum at an energy level where the shell region has a zero-valued dispersive mass. A realistic design of the heterostructure based on the $Hg_{1-x}Cd_xTe$ compound has been proposed. An in-depth analysis of the suggested heterostructure, based on the envelope function formalism, has been presented, showing the possibility to trap an electron within the resonator core. The trapping lifetime of a detuned heterostructure has also been characterized, and it has been shown that the heterostructure can trap the electron for a long time, even if there is slight detuning. Finally, we investigated the possibility of a free electron being captured by the semiconductor resonator. Notably, our analysis has revealed that, in the same manner as a trapped electron is unable to escape from the resonator, a free electron cannot be permanently captured by the resonator. Interestingly, the scattering cross section does not exhibit any resonant features for a perfectly tuned structure. This confirms that a free electron is unable to interact with the embedded bound energy eigenstate.

Although it is challenging to capture the incident electron within the core of an ideal structure, our future aim will be to

investigate how to couple the electron to the embedded bound state, e.g., by a temporary detuning of the heterostructure. Moreover, due to the effective-medium approximation, another aim is to confirm the results with first-principles calculations of the electronic band structure.

APPENDIX

In the Supplemental Material of Ref. [33] it is formally demonstrated that, within an effective-medium framework, the relation between the spatially averaged probability density associated with a Bloch energy eigenstate and the macroscopic wave function is such that

$$\langle |\psi_{mic}|^2 \rangle = \left(1 - \frac{\partial \hat{H}_{eff}}{\partial E} \right) |\psi_{eff}|^2. \qquad (A1)$$

In the above equation, $\hat{H}_{eff}(E, \mathbf{k})$ represents the homogenized (energy-dependent) Hamiltonian with $\mathbf{k} = -i\nabla$. In this paper, the effective-medium Hamiltonian is given by [see Eq. (3)]

$$\hat{H}_{eff}(E, \mathbf{k}) = \frac{\hbar^2 k^2}{2m} + V_{eff}. \qquad (A2)$$

Hence, it follows that

$$\langle |\psi_{mic}|^2 \rangle = \left(1 - \frac{\partial V_{eff}}{\partial E} \right) |\psi_{eff}|^2 - \frac{\partial}{\partial E} \left(\frac{1}{m} \right) \frac{\hbar^2}{2} |i\mathbf{k}\psi_{eff}|^2. \qquad (A3)$$

For a Bloch energy eigenstate in a continuous medium, we have $i\mathbf{k}\psi_c = \nabla\psi_c$, and thus the above result leads to Eq. (2) of the main text.

[1] K. Gottfried and T.-M. Yan, *Quantum Mechanics: Fundamentals*, 2nd ed. (Springer, Berlin, 2003).

[2] J. von Neumann and E. Wigner, Über merkwürdige diskrete eigenwerte, Phys. Z. **30**, 465 (1929).

[3] F. H. Stillinger and D. R. Herrick, Coherent potential approximation: Basic concepts and applications, Phys. Rev. A **11**, 446 (1975).

[4] E. N. Bulgakov, K. N. Pichugin, and I. Rotter, Bound states in the continuum in open Aharonov-Bohm ring, JETP Lett. **84**, 430 (2006).

[5] A. F. Sadreev, E. N. Bulgakov, and I. Rotter, Bound states in the continuum in open quantum billiards with a variable shape, Phys. Rev. B **73**, 235342 (2006).

[6] N. Moiseyev, Suppression of Feshbach Resonance Widths in Two-Dimensional Waveguides and Quantum Dots: A Lower Bound for the Number of Bound States in the Continuum, Phys. Rev. Lett. **102**, 167404 (2009).

[7] H. Feshbach, Unified theory of nuclear reactions, Ann. Phys. (NY) **5**, 357 (1958).

[8] R. G. Newton, *Scattering Theory of Waves and Particles*, 2nd ed. (Springer, Berlin, 2013).

[9] H. Friedrich and D. Wintgen, Interfering resonances and bound states in the continuum, Phys. Rev. A **32**, 3231 (1985).

[10] H. Nakamura, N. Hatano, S. Garmon, and T. Petrosky, Quasi-bound States in the Continuum in a Two Channel Quantum Wire with an Adatom, Phys. Rev. Lett. **99**, 210404 (2007).

[11] F. Capasso, C. Sirtori, J. Faist, D. L. Sivco, S.-N. G. Chu, and A. Y. Cho, Observation of an electronic bound states above a potential well, Nature (London) **358**, 565 (1992).

[12] T. A. Weber, Bound states with no classical turning points in semiconductor heterostructures, Solid State Commun. **90**, 713 (1994).

[13] A. Albo, D. Fekete, and G. Bahir, Electronic bound states in the continuum above (Ga, In)(As, N)/(Al, Ga)As quantum wells, Phys. Rev. B **85**, 115307 (2012).

[14] N. A. Gippius, S. G. Tikhodeev, and T. Ishihara, Optical properties of photonic crystal slabs with an asymmetrical unit cell, Phys. Rev. B **72**, 045138 (2005).

[15] A. G. Borisov, F. J. García de Abajo, and S. V. Shabanov, Role of electromagnetic trapped modes in extraordinary transmission in nanostructured materials, Phys. Rev. B **71**, 075408 (2005).

[16] D. C. Marinica, A. G. Borisov, and S. V. Snabanov, Bound States in the Continuum in Photonics, Phys. Rev. Lett. **100**, 183902 (2008).

[17] M. G. Silveirinha, Trapping light in open plasmonic nanostructures, Phys. Rev. A **89**, 023813 (2014).

[18] F. Monticone and A. Alu, Embedded Photonic Eigenvalues in 3*d* Nanostructures, Phys. Rev. Lett. **112**, 213903 (2014).

[19] Y. Plotnik, O. Peleg, F. Dreisow, M. Heinrich, S. Nolte, A. Szameit, and M. Segev, Experimental Observation of Optical Bound States in the Continuum, Phys. Rev. Lett. **107**, 183901 (2011).

[20] J. Lee, B. Zhen, S.-L. Chua, W. Qiu, J. D. Joannopoulos, M. Soljacic, and O. Shapira, Observation and Differentiation of Unique High-*Q* Optical Resonances Near Zero Wave Vector in Macroscopic Photonic Crystal Slabs, Phys. Rev. Lett. **109**, 067401 (2012).

[21] Ch. W. Hsu, B. Zhen, J. Lee, S.-L. Chua, S. G. Johnson, J. D. Joannopoulos, and M. Soljacic, Observation of trapped light within the radiation continuum, Nature (London) **499**, 188 (2013).

[22] L. Golstone and A. A. Oliner, Leaky-wave antennas i: Rectangular waveguides, IEEE Trans. Antennas Propag. **7**, 307 (1959).

[23] S. Monticone and A. Alu, Leaky-wave theory, techniques, and applications: From microwaves to visible frequencies, Proc. IEEE **103**, 793 (2015).

[24] G. Bastard, *Wave Mechanics Applied to Semiconductor Heterostructures* (Wiley, New York, 1988).

[25] H. S. Friedrich, *Theoretical Atomic Physics* (Springer, Berlin, 2006).

[26] E. O. Kane, Band structure of indium antimonide, J. Phys. Chem. Solids **1**, 249 (1957).

[27] G. Bastard and J. A. Brum, Electronic states in semiconductor heterostructures, IEEE J. Quantum Electron. **22**, 1625 (1986).

[28] M. G. Silveirinha and N. Engheta, Effective medium approach to electron waves: Graphene superlattices, Phys. Rev. B **85**, 195413 (2012).

[29] S. Lannebère and M. G. Silveirinha, Effective Hamiltonian for electron waves in artificial graphene: A first-principles derivation, Phys. Rev. B **91**, 045416 (2015).

[30] M. G. Silveirinha and N. Engheta, Transformation electronics: Tailoring the effective mass of electrons, Phys. Rev. B **86**, 161104 (2012).

[31] M. G. Silveirinha and N. Engheta, Metamaterial-inspired model for electron waves in bulk semiconductors, Phys. Rev. B **86**, 245302 (2012).

[32] G. Bastard, Theoretical investigations of superlattice band structure in the envelope-function approximation, Phys. Rev. B **25**, 7584 (1982).

[33] D. E. Fernandes, N. Engheta, and M. G. Silveirinha, Wormhole for electron waves in graphene, Phys. Rev. B **90**, 041406(R) (2014).

[34] G. B. Arfken and H. J. Weber, *Mathematical Methods for Physicists*, 5th ed. (Harcourt/Academic, San Diego, 2001).

[35] C. A. Balanis, *Antenna Theory: Analysis and Design*, 2nd ed. (Wiley, New York, 1997).

[36] L. Jelinek, J. D. Baena, J. Voves, and R. Marques, Metamaterial-inspired perfect tunneling in semiconductor heterostructures, New J. Phys. **13**, 083011 (2011).

[37] T. K. Gaylord, G. N. Henderson, and E. N. Glytsis, Application of electromagnetics formalism to quantum-mechanical electron-wave propagation in semiconductors, J. Opt. Soc. Am. B **10**, 333 (1993).

[38] D. Dragoman and M. Dragoman, Optical analog structures to mesoscopic devices, Prog. Quantum Electron. **23**, 131 (1999).

[39] D. Dragoman and M. Dragoman, Metamaterials for ballistic electrons, J. Appl. Phys. **101**, 104316 (2007).

[40] G. L. Hansen, J. L. Schmitt, and T. N. Casselman, Energy gap versus alloy composition and temperature in $Hg_{1-x}Cd_xTe$, J. Appl. Phys. **53**, 7099 (1982).

[41] A. Rogalski, HgCdTe infrared detector material: History, status and outlook, Rep. Prog. Phys. **68**, 2267 (2005).

[42] S. P. Kowalczyk, J. T. Cheung, E. A. Kraut, and R. W. Grant, CdTe-HgTe (111) Heterojunction Valence-Band Discontinuity: A Common-Anion-Rule Contradiction, Phys. Rev. Lett. **56**, 1605 (1986).

[43] J. D. Wiley and R. N. Dexter, Helicons and nonresonant cyclotron absorption in semiconductors. ii. $Hg_{1-x}Cd_xTe$, Phys. Rev. **181**, 1181 (1969).

[44] M. G. Silveirinha and N. Engheta, Giant nonlinearity in zero-gap semiconductor superlattices, Phys. Rev. B **89**, 085205 (2014).

[45] N. W. Aschroft and N. D. Mermin, *Solid State Physics* (Holt, Rinehart and Winston, New York, 1976).

[46] J. D. Jackson, *Classical Electrodynamics*, 3rd ed. (Wiley, New York, 1998).

[47] P. M. Morse and H. Feshbach, *Methods of Theoretical Physics* (McGraw-Hill, New York, 1953).